Journal of Power Sources 196 (2011) 69–75

Contents lists available at ScienceDirect

Journal of Power Sources

journal homepage: www.elsevier.com/locate/jpowsour

Ultrahigh figure-of-merit for hydrogen generation from sodium borohydride using ternary metal catalysts

Lunghao Hu [a,b,*], R. Ceccato [a], R. Raj [b]

[a] Department of Materials Engineering and Industrial Technologies, University of Trento, Via Mesiano 77, 38050, Italy
[b] Department of Mechanical Engineering, University of Colorado, Boulder, CO 80309-0427, USA

ARTICLE INFO

Article history:
Received 8 July 2010
Accepted 10 July 2010
Available online 17 July 2010

Keywords:
Ternary catalyst
Carbon nanotube support
Sodium borohydride
Hydrogen generation
Silicon carbonitride
Polymer-derived-ceramics

ABSTRACT

We report further increase in the figure-of-merit (FOM) for hydrogen generation from $NaBH_4$ than reported in an earlier paper [1], where a sub-nanometer layer of metal catalysts are deposited on carbon nanotube paper (CNT paper) that has been functionalized with polymer-derived silicon carbonitride (SiCN) ceramic film. Ternary, Ru–Pd–Pt, instead of the binary Pd–Pt catalyst used earlier, together with a thinner CNT paper is shown to increase the figure-of-merit by up to a factor of six, putting is above any other known catalyst for hydrogen generation from $NaBH_4$. The catalysts are prepared by first impregnating the functionalized CNT-paper with solutions of the metal salts, followed by reduction in a sodium borohydride solution. The reaction mechanism and the catalyst efficiency are described in terms of an electric charge transfer, whereby the negative charge on the BH_4^- ion is exchanged with hydrogen via the electronically conducting SiCN/CNT substrate [1].

1. Introduction

Metal hydrides possess a high capacity for hydrogen storage [2]. Among these compounds, sodium borohydride yields pure hydrogen upon hydrolysis, and the rate of hydrogen generation can be controlled with the use of a catalyst [3–5]. $NaBH_4$ is a prime candidate for fuel cells that can operate at ambient temperatures, e.g. proton exchange membrane cells (PEMFC) [6,7]. A catalyst is necessary to overcome the gradual loss of generation rate with the production of $NaBO_2$ following the overall reaction: $NaBH_4 + 2H_2O \rightarrow NaBO_2 + 4H_2$, which renders the solution increasingly basic with hydrogen evolution [8,9]. Controlled production of hydrogen is therefore obtained by buffering the solution at high pH and then using catalysts, belonging to the transition metal-based compounds: among them, metal salts, metal borides, and precursors of metal oxides [10–12]. Metal nanoparticles, with large surface area, increase the catalytic activity [13–15]. In earlier work [1] it has been shown that CNT paper functionalized with a film of a polymer-derived SiCN can disperse the transition metals deposited on its surface supposedly into a monolayer, thereby increasing the figure-of-merit (FOM), expressed as the rate of hydrogen generation per unit weight of the metal (per unit molar concentration of $NaBH_4$) for the catalyst.

In this earlier paper [1], a binary catalyst (Pt–Pd) was used. Here we show that a ternary catalyst constituted from Pt–Pd–Ru enhances the catalytic efficiency. A thinner CNT paper substrate is shown to further increase the catalytic activity, presumably by reducing the likelihood of hydrogen bubbles becoming trapped within the paper. Overall, up to *six-fold* increase in the FOM is achieved, placing this catalyst above any known catalyst for hydrogen generation from $NaBH_4$.

In the present work the ternary metal catalyst was prepared by reverse micellar solutions in cyclohexane. Triton X-100 and 2-propanol were used as the surfactant and the co-surfactant to stabilize the suspension. The SiCN-functionalized CNT paper was impregnated with this suspension. The salts were reduced into elemental metals in the sodium borohydride solution, which acted by itself as a reducing agent [16–19] thus simplifying the process for catalyst manufacture. The new results are compared to earlier publications with the single and binary metal catalyst with different substrates [1,20–28]. These studies have considered the noble metals deposited on different substrates. Kojima worked on Pt catalyst deposited on TiO_2 by a supercritical method, which provided a high FOM [20]. Krishanan has studied binary catalyst Pt–Ru, as well as single Pt and Ru catalysts deposited on $LiCoO_2$ substrate [23]. Pd–C powder and thin film Pd catalysts have been explored by Patel [21]. Peña-Alonso et al. made a carbon nanotube paper for the catalyst support with binary catalyst Pt/Pd [1]. Demirci was interested in Ru catalyst coated on sulphated zironica substrate [22]. Other research groups have worked on the non noble metal catalysts, Co and Ni, for hydrogen generation to reduce cost. For example, Ye et al. exam-

* Corresponding author at: Department of Mechanical Engineering, University of Colorado, Boulder, CO 80309-0427, USA.
Tel.: +1 303 735 2651; fax: +1 303 492 3498.
E-mail addresses: lunghao.hu@gmail.com, lung.hu@colorado.edu (L. Hu).

0378-7753/$ – see front matter © 2010 Elsevier B.V. All rights reserved.
doi:10.1016/j.jpowsour.2010.07.037

Table 1
The comparison of FOM between Pt–Pd–Rd/SiCN/CNT paper and other references.

Catalyst	Catalyst support	Temperature	[$NaBH_4$]	FOM ($l\,min^{-1}\,[NaBH_4]^{-1}\,g_{met}^{-1}$)	Reference
Pt/Pd/Ru	25 μm thick SiCN/CNT paper	29 °C	0.03 M (1 M NaOH)	920	Present work
					Present work
					Present work
					Present work
					Present work
					Present work
Pt/Pd/Ru	75 μm thick SiCN/CNT paper	29 °C	0.03 M (1 M NaOH)	730	
Pt/Pd/Ru	150 μm thick SiCN/CNT paper	29 °C	0.03 M (1 M NaOH)	390	
Ru/Pd	25 μm thick SiCN/CNT paper	29 °C	0.03 M (1 M NaOH)	490	
Pt/Pd	25 μm thick SiCN/CNT paper	29 °C	0.03 M (1 M NaOH)	470	
Pt/Ru	25 μm thick SiCN/CNT paper	29 °C	0.03 M (1 M NaOH)	650	
Pt/Pd	150 μm thick SiCN/CNT paper	29 °C	0.03 M (1 M NaOH)	175	[1]
Pt	TiO_2	20–23 °C	50 mg $NaBH_4$, 5 g H_2O	400	[20]
Pt	Activated carbon	20–23 °C	50 mg $NaBH_4$, 5 g H_2O	90	[20]
Pd	Carbon powder	297 K	0.005 M $NaBH_4$	185	[21]
Ru	Sulphated zironia	24 °C	0.529 M $NaBH_4$ (1 M NaOH)	13.6	[22]
Pt/Ru	$LiCoO_2$	25 °C	5 wt% $NaBH_4$, 5 wt% NaOH	12.9	[23]
Ru	$LiCoO_2$	25 °C	5 wt% $NaBH_4$, 5 wt% NaOH	7.1	[23]
Pt	$LiCoO_2$	25 °C	5 wt% $NaBH_4$, 5 wt% NaOH	4.3	[23]
Co50/Raney Ni50	None	293 K	1 g $NaBH_4$, 100 ml H_2O	2.3	[24]
Co-B	None	30 °C	20 wt% $NaBH_4$, 5 wt% NaOH	0.5	[25]
Co	γ-Al_2O_3	30 °C	5 wt% $NaBH_4$, *x* wt% NaOH	0.2	[26]
Co/filamentary Ni	Ni foam	30 °C	10 wt% $NaBH_4$, 0.01 M KOH	0.05	[27]
Ru	Graphite powder	30 °C	10 wt% $NaBH_4$, 5 wt% NaOH	12.24	[28]
Ru	Graphite powder	30 °C	5 wt% $NaBH_4$, 1 wt% NaOH	17.74	[28]

ined Co metal deposited on γ-Al_2O_3 [26]. Jeong used Co–B powder as the catalyst directly to react with sodium borohydride [25]. Liu used Raney Ni50–Co50 as the catalyst [24].

The present work is distinguished from the above reports in that ≪1 ppm loadings of the precious metals are shown to yield very high catalytic efficiency, leading to a higher figure-of-merit (FOM) than for any other known catalyst. The FOM values obtained in the current work are compared to those published in the literature in Table 1. The cost implications of the findings reported here are self-evident.

The FOM is defined as $l\,min^{-1}\,[NaBH_4]\,g_{met}^{-1}$, that is, the rate of hydrogen generation per unit molar concentration of $NaBH_4$, per gm weight of the precious metal. The factors influencing the FOM are complex. They can be correlated to the cluster size of the metal [29,30] the composition of the metal alloys [30–39] and the interaction between the metals, ligands and substrates [33,39]. The properties of the substrate, such as its electronic conductivity and surface area, can substantially influence the catalytic efficiency (FOM) [13–15,35–42]. SiCN/CNT paper combines a very high surface area with electronic conductivity, permitting electron transfer mechanisms between different sites on the catalyst surface for hydrogen generation.

2. Experimental methods

2.1. Catalyst preparation

The SiCN/CNT paper was prepared by sonicating a fixed weight amount of single wall carbon nanotube (SWNT; Purified HiPco Single wall carbon nanotubes, Unidym, Houston, TX) in deionized water with the presence of Triton X-100 (Sigma–Aldrich, St. Louis, MI) as a surfactant. The thickness in the final SWNT paper was controlled by the weight of the CNTs added to the suspension (for example, 25 mg of SWNT would make ∼150 μm thick paper, whereas 4 mg of SWNT can make ∼25 μm thick paper). Then the SWNT suspension was filtered with 5 μm filter paper in a device made with an Erlenmeyer flask connected to a water vacuum pump; a Gooch filter was inserted on the top of the flask, sealed with a rubber o-ring. After filtering, the SWNT paper was rinsed with acetone, methanol, and ethanol and deionized water in order to remove most of surfactant. Then, the SWNT paper was heat-treated at 1100 °C for three hours under argon gas flow to burn out the residual surfactant. Finally, the SWNT paper was dip-coated with 10 wt% commercially polyureamethylvinylsilazane polymeric precursor (Ceraset^{TM}-SN from KiON Corp., Wiesbaden, Germany) diluted by acetone [43]. After drying out the solvent, the SWNT paper was cross-linked at 300 °C for 1 h and then pyrolyzed at 1100 °C for 3 h under argon gas flow. A SiCN film was formed on the surface of SWNT paper.

Catalysts were prepared by the following procedure reported in the literature [13,16–18,43–45]. The metal ionic solutions were prepared by using chloroplatinic acid hexahydrate 40 mM solution, ($H_2PtCl_6{\cdot}6H_2O$, ABCR), acidic (40 ml of 1 M HCl and 60 ml of deionized water) $PdCl_2$ 40 mM (ABCR) solution, and $RuCl_3{\cdot}xH_2O$ (ABCR) 20 mM solution. The preparation of nanoparticles was performed by a two-emulsion technique. Each microemulsion system consisted of Triton X-100 as a surfactant, 2-propanol as a co-surfactant, and cyclohexane as the continuous oil phase; the Pt–Pd–Ru solutions and sodium borohydride aqueous solution represented the dispersed aqueous phases. The volume ratio of each microemulsion system was obtained by mixing 40 ml of cyclohexane, 20 ml of 2-propanol, 4 ml of Triton X-100; then, 1 ml of each metal ionic solution and 1 ml of 1 M sodium borohydride aqueous solution were added drop-by-drop into each microemulsion [46,47]. After homogenization, SiCN/CNT paper was immersed into metal ionic emulsion for impregnation under slow stirring in order to prevent the SiCN/CNT paper from breaking. Then, 2 ml of sodium borohydride emulsion were added to reduce the metal particles. Finally, the solution was filtered out to recover the catalyzed SiCN/CNT paper samples, which were rinsed with ethanol and deionized water to remove the residual stabilizer. These samples were then ready as catalysts for hydrogen generation experiments.

2.2. Hydrogen generation measurements

All experiments were performed at ambient pressure and at a temperature of 29–30 °C, fixed by a water thermostat. A two-neck reaction flask, into which the catalyst sample had been previously inserted, was connected on the one side to a burette filled with dye water, and on the other side to a gas valve for syringe injection

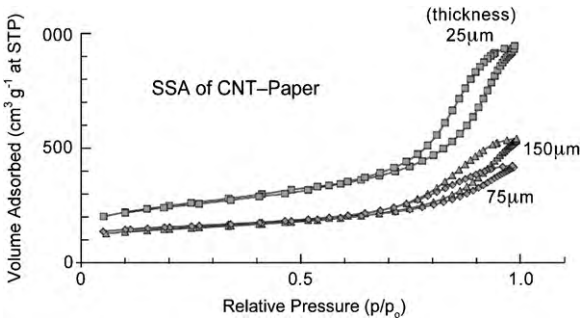

Fig. 1. Nitrogen adsorption/desorption isotherms of CNT papers with different thicknesses.

of the reactant solution. The sodium borohydride solution (0.03 M) was prepared with 1 M NaOH solution. A fixed volume, 8 ml, of this solution was poured into the reaction flask. Each run used 5 mg of catalyzed SiCN/CNT paper. After a quick injection of the sodium borohydride solution, the gas valve was closed immediately. The solution was stirred at 900 rpm. The volume of evolved hydrogen gas was measured as a function of time, by change in the dye level in the burette.

2.3. Characterization

Nitrogen physisorption measurements were performed on a Micromeritics ASAP 2010 instrument. Samples were degassed below 1.3 Pa prior to the analysis. Both adsorption and desorption branches were recorded with a fixed equilibration time of 20 s for each measured point. Specific surface area (SSA) of the samples was evaluated with the BET equation within the relative pressure range: $0.05 \leq p/p_0 \leq 0.33$.

X-ray diffraction (XRD) spectra were collected on a Rigaku D-Max III diffractometer in the Bragg-Brentano geometry, using Cu Kα radiation and a graphite monochromator in the diffracted beam. Scans of SiCN/CNT paper and catalyst-impregnated samples were recorded within the range 10–70° in 2θ values. Elemental analysis of the metal catalysts was obtained by inductively coupled plasma ICP-OES Ciros Spectro instrument. Selected wavelengths for metals were selected at 214.423 nm (Pt), 340.458 nm (Pd) and 240.272 nm (Ru). Weighted fragments of SiCN/CNT papers with metals were dissolved in "aqua regia" (HCl/HNO_3 3/1, v/v) solutions and then analyzed.

Transmission electron microscopy (TEM) observations were carried out with a Philips 400 T microscope, operating at 120 kV and equipped with an EDAX energy dispersive X-ray spectrometer for elemental mapping. The samples were prepared by sonicating pieces of catalyzed SiCN/CNT paper in ethanol for few minutes and then few drops of the resulting suspensions were poured on the copper grid covered with a carbon film and a survey scan of XPS had been used to characterize the Pt–Pd–Ru coated SiCN/CNT paper (Fig. 1).

3. Results and discussion

3.1. Sample characterization

All SiCN/CNT samples showed Type II-b physisorption isotherms, according to the IUPAC classification. The presence of an H4-type hysteresis loop, joined to the absence of a plateau region at higher relative pressure values, could be attributed to the presence of plate-like particles and slit-shaped micropores [47,48]. From the evaluation of the adsorption curve with the BET equation, specific surface area (SSA) values range from 470 to 860 $m^2 g^{-1}$, depending on the thicknesses of the samples, were calculated. The

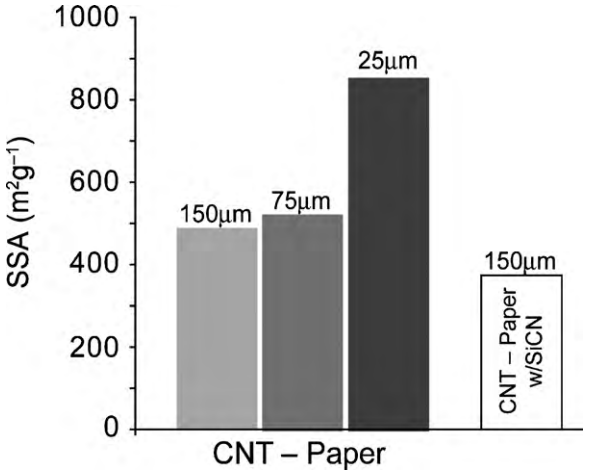

Fig. 2. Specific surface area with different thicknesses of CNT and SiCN/CNT papers.

SSA measurements for CNT papers 150, 75 and 25 μm thick are given in the bar chart in Fig. 2. The SiCN coated 150 μm paper shows a slight reduction in the SSA as would be expected from the deposition of a SiCN layer on the nanotubes.

The metal weight in the catalysts was obtained from elemental analysis, performed by ICP-OES. This analysis gave the following results: 0.63 wt% for Pt, 0.165 wt% for Pd and 0.07 wt% for Ru in the 150 μm thick sample; 0.21 wt% for Pt, 0.17 wt% for Pd and 0.69 wt% for Ru in the 75 μm thick paper, and 0.81 wt% for Pt, 0.059 wt% for Pd and 0.26 wt% for Ru in the 25 μm thick paper. Note that the total weight of the catalyst in the experiments was kept constant at 5 mg. The metal content in this catalyst was determined from the overall percentage of the metal constituents measured by ICP. The FOM was determined by normalizing the measured rate of hydrogen generation against the metal content in the 5 mg samples. The survey scan of XPS of the 75 μm catalyst is given in Fig. 3. The atom ratio of Pt to Pd is 0.43. Pd_{3d} and Pt_{4f} have binding energies, 67.7 and 335.2 eV. Unfortunately the Ru_{3d} peak overlaps the C_{1s} peak making it difficult to detect Ru. The atomic ratio of Pt/Pd converted to weight ratio is 0.82, compared to the ratio of Pt/Pd, 1.2, from ICP elemental analysis of 75 μm catalyst. The ratio of Pt/Pd is comparable between XPS and ICP.

The XRD spectrum from the catalyst is shown in Fig. 4. The absence of definitive peaks suggests that the metal catalyst was not present in the form of (nano)crystalline particles. (When some of

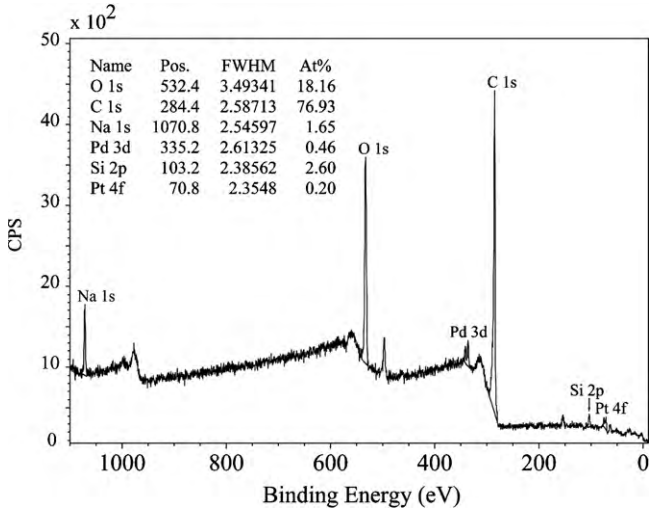

Fig. 3. XPS spectra of Pt/Pd/Ru catalyzed SiCN/CNT paper.

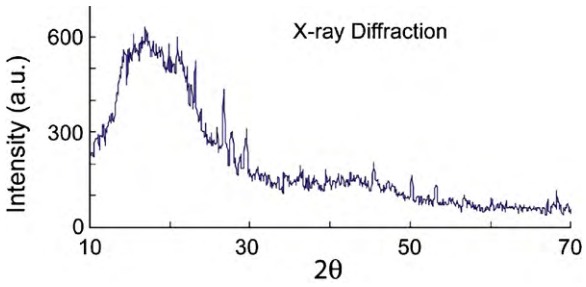

Fig. 4. XRD spectra of Pt/Pd/Ru catalyst deposited on 150 μm thick SiCN/CNT paper.

the platinum atoms in the fcc crystal structure are replaced by other metallic atoms, like Ru and Pd, the diffraction peaks shift slightly to higher angles [45,49,50–52].) These diffraction peaks would be expected to present at 40°, 46° and 68° that are ascribed to (1 1 1), (2 0 0) and (2 2 0) planes of fcc crystals of the nanoparticles. While it is possible that the metal content in the samples was not enough to yield a measureable diffraction peak, the TEM results given below, also, do not support the presence of nanoparticles of the metals on the catalyst surface.

The dispersion of the metal atoms on the SiCN-CNT substrate was further studied by comparing the TEM micrographs from the SiCN coated substrate, and from metals deposited directly on to a carbon film. These micrographs are compared in Fig. 5. While the SiCN-CNT sample (Fig. 5, top) is featureless, the metals deposited on carbon film (Fig. 5, bottom) – prepared in the same way as the

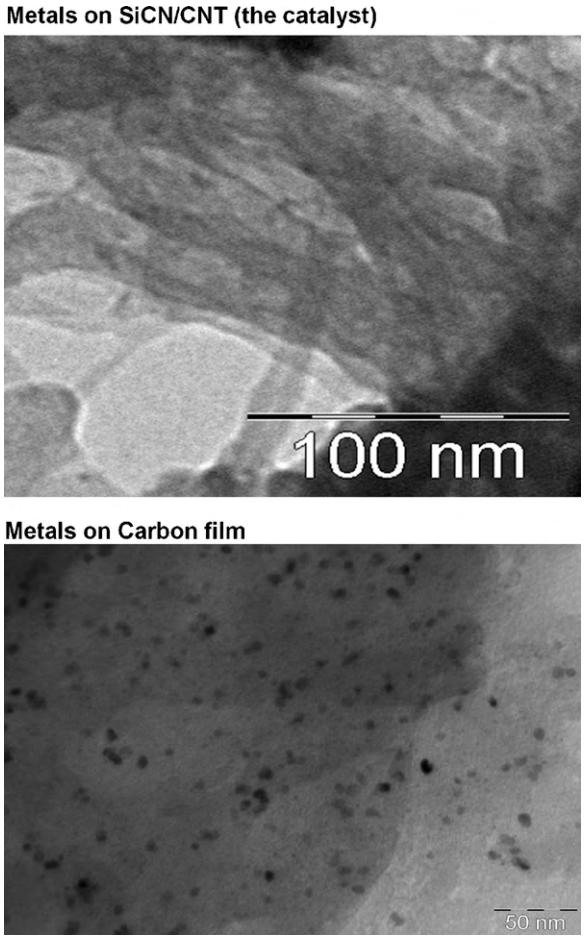

Fig. 5. (Top) TEM micrograph of Pt/Pd/Ru catalyst deposited on filtered SiCN/CNT paper. (Bottom) TEM micrograph of the ternary Pt/Pd/Ru catalyst deposited on a carbon film.

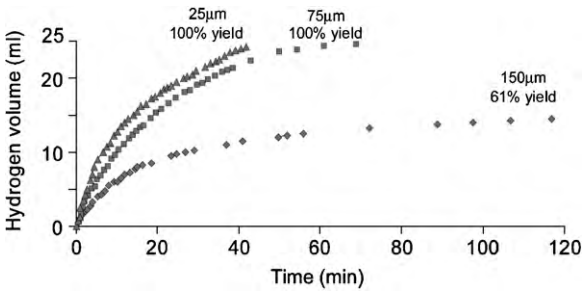

Fig. 6. The generation volume of hydrogen employing ternary catalysts of different thicknesses.

catalyst – show the presence of nanoparticles of the metal ranging from 4 to 8 nm in diameter. These micrographs suggest that the metal atoms in the SiCN-CNT catalyst may indeed have been dispersed as a sub-nanometer layer. This point is discussed in Ref. [1], where the high affinity of transition metals with Si, with which they form strongly bonded silicides, is given as the possible reason for the monolayer dispersion of the metal on SiCN-CNT surfaces. The strong bonds would inhibit diffusion on the surface that would be necessary for coalescence of the metal atoms into nanoparticles.

The SiCN coated CNT paper is electronically conductive. Earlier experiments have shown that SiCN layer on CNT paper enhances the supercapacity and the electro-chemico-mechanical actuation behavior of CNT [43].

3.2. Influence of CNT paper thickness

Experiments were carried out with catalysts made with three different thicknesses of the CNT paper: 150, 75, and 25 μm. The relative performance of these catalysts was measured using the same weight of the catalyst (5 mg), immersed in 8 ml of 0.03 M solution of $NaBH_4$. The theoretical volume of hydrogen that is available at STP (25 °C, 1 atm) from this solution is equal to 23.5 ml. At this concentration of $NaBH_4$, the hydrogen generation kinetics is predominantly first order [1].

The data for time dependent hydrogen generation from the above three samples are given in Fig. 6. While the 75 and 25 μm samples do indeed yield the theoretical volume of hydrogen, within about 1 h, the 150 μm sample reaches only 61% yield after 2 h. A likely explanation is that the hydrogen bubbles generated in the 150 μm sample became trapped in the CNT network, thus greatly reducing the efficiency of the catalyst. Thus early on, that is within the first 10 min; the hydrogen could have been released more easily than later on when the trapped bubbles greatly slowed further activity of the catalyst.

3.3. Catalyst efficiency: the figure-of-merit (FOM)

The FOM for the catalysts is defined as rate of hydrogen generation per unit molar concentration of $NaBH_4$ per unit weight of the metal. It is expressed in units of $l\,min^{-1}\,g_{met}{}^{-1}[NaBH_4]^{-1}$. The rate is equal to the initial rate of hydrogen generation, which occurs at $[NaBH_4] = 0.03$ molar, that is, at the initial concentration of the solution in the experiment. This initial rate *may* be calculated from the slope of the hydrogen generation curve in the first 5–10 min of the experiment: the same procedure that was used in Ref. [1]. However, as shown below this method is rather approximate. Later on the hydrogen production curve is fitted to a first order kinetic equation, which gives a more reliable value for the initial rate of hydrogen production.

The hydrogen generation data, for the first 10 min, for the specimens of three thicknesses are shown in Fig. 7 (left). The data from Ref. [1] is given as the benchmark. The initial slopes of these data

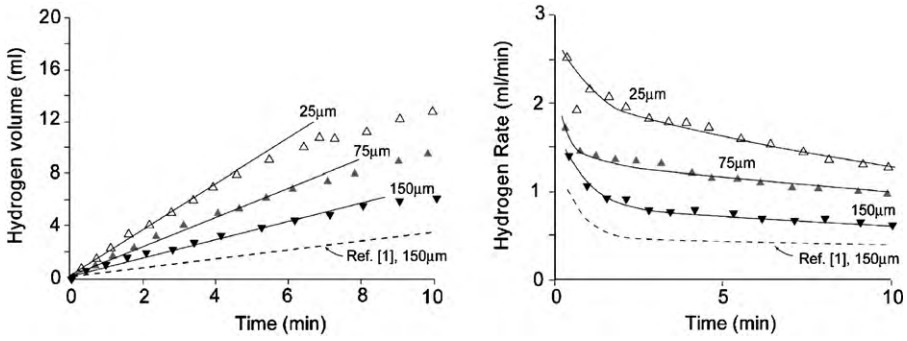

Fig. 7. (Left) Hydrogen generation during the first 10 min of the experiment. (Right) The rate of hydrogen generation during the first 10 min.

sets give the following values for the hydrogen generation rate: 0.70, 1.15 and 1.8 ml min^{-1} for specimens having the thickness of 150, 75 and 25 μm, respectively. The benchmark data from Ref. [1], which also used a 150 μm sample gave a rate of 0.35 ml min^{-1} (this lower value in comparison to the present work is attributed to the ternary, instead of the binary [1,23,24] catalyst). The thinner catalysts have higher rates. The correlation between hydrogen generation rate and sample thickness is likely from the trapping of hydrogen bubbles within the CNT network in the samples (this was the starting hypothesis that spurred the study of the thickness effect on hydrogen generation).

As seen in Fig. 7(left) the rate of hydrogen generation starts to decline during the first 10 min. This result is made clear in Fig. 7(right) where the instantaneous slope of the curves is plotted against time. While there is a change in the absolute values the relative magnitudes of the rates for the samples of different thicknesses remains as discussed above.

In order to obtain a value for the FOM, in units of l min^{-1} $gmet^{-1}[NaBH_4]^{-1}$, it is necessary to determine the initial value of the generation rate, R_o. This is accomplished by fitting the data to a first order equation, given by,

$$H = H_o(1 - e^{t/\tau}) \quad (1)$$

where H is the time dependent volume of hydrogen generated in the experiment, H_o is the theoretical limit, and τ is the first order rate constant. The fit for Eq. (1) to the data for the 75 μm thick specimen is shown in Fig. 8. The fit gives the values for H_o and τ. The initial rate is obtained by differentiating Eq. (1) and setting $t \to 0$, which gives that:

$$R_o = \frac{H_o}{\tau} \quad (2)$$

Inserting the values for R_o for the three specimens in this way into the equation for the FOM, we obtain the results that are given in Fig. 9. Note that the 25 μm sample has the highest FOM, reaching 900 l min^{-1} $g_{met}{}^{-1}[NaBH_4]^{-1}$, which is nearly six times greater than the benchmark value obtained in Ref. [1] and much high than the papers published [20–28], as listed in Table 1.

The influence of binary vs. the ternary metal compositions on the FOM is shown in Fig. 10. The ternary composition is based upon Pt–Pd–Ru. The binary compositions consider the three possible combinations, Pt–Pd, Ru–Pd, and Pt–Ru. In all instances the ternary composition gives a value for the FOM that is at least 50% greater than for the binary compositions. It is difficult to give a definitive reason as to why the ternary compositions perform better without conducting *ab initio* molecular dynamics calculations. In general terms though, it can be expected the use of different elements, especially in monolayer configurations, can create a more diverse distribution of energy levels in the electronic structure which would tend to promote the charge transfer mechanism for the catalytic behavior, as discussed in [1].

4. Summary

The single wall carbon nanotubes, functionalized with a polymer-derived silicon-carbonitride based coating, serves as an effective support for metallic dispersions (Pt, Pd and Ru). These ternary compositions yield a FOM of

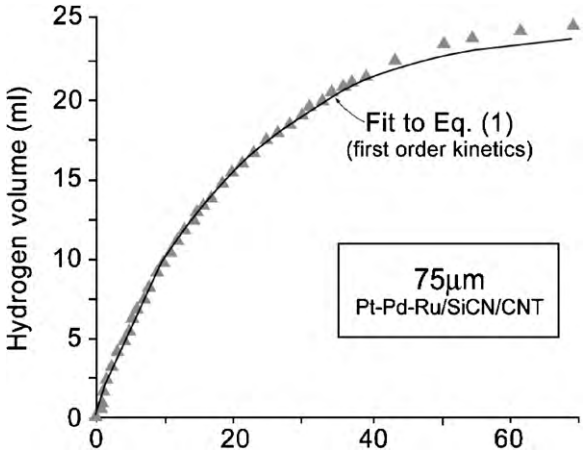

Fig. 8. The fit of first order kinetics (Eq. (1)) to the data for 75 μm SiCN/CNT ternary catalyst.

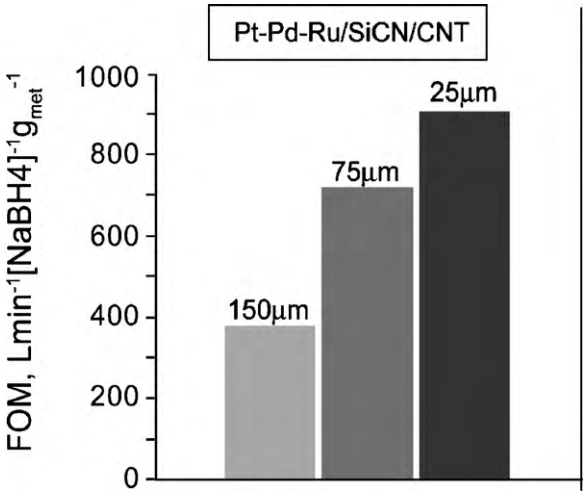

Fig. 9. The FOM for catalyst of different thicknesses.

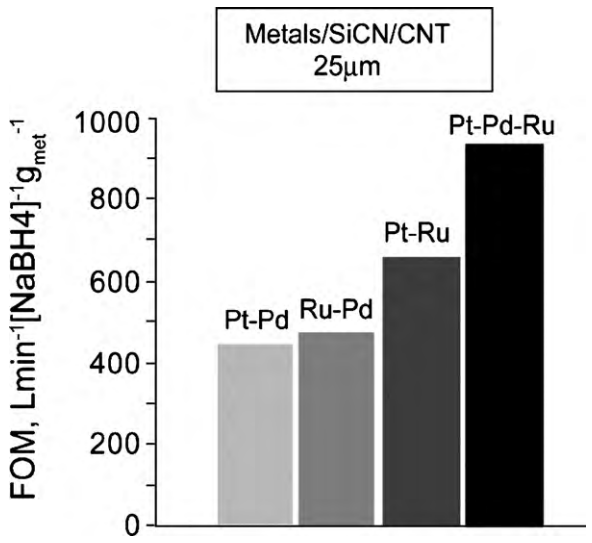

Fig. 10. The FOM of catalyst with different combinations of binary compositions and ternary composition – all for the thickness of 25 μm.

$\sim$900 l min^{-1} $g_{met}{}^{-1}$[$NaBH_4$]$^{-1}$, for hydrogen generation, the highest value reported in the literature. The ternary compositions yield an FOM that is 150% of the value obtained with binary compositions.

The hydrogen generation rate is also influenced by the thickness of the CNT paper that is used as the basic substrate for the preparation of the catalyst: thinner substrates are better, presumably since they reduce the chance of trapping hydrogen bubbles within the CNT network. The minimum thickness of the substrates in these experiments (25 μm) was limited by the physical fragility of the substrates; thinner substrates were difficult to handle without breaking them. The thinner CNT paper has higher specific surface area that provides more uniform coating of metals and increases the surface to volume ratio, which can be an alternative explanation for the higher catalytic activity of the of the 25 μm CNT paper.

The electronically conducting SiCN/CNT substrate provides a pathway for electron transfer from $BH_4{}^-$ ion: the negative charge on $BH_4{}^-$ ion is transferred to one hydrogen atom, which is reduced by water molecules in $NaBH_4$ hydrolysis. It is possible that the different electron chemical potential of the metal atoms facilitates the catalytic activity. Apparently the metal is deposited as a monolayer on the substrate: this geometry can modify the electronic structure relative to "bulk" metal particles due to quantum confinement. The bridging of the energy levels in the electronic structure may allow the valence and conduction bands in the metal atoms to connect or overlap. This overlap can then facilitate the electron transfer on $BH_4{}^-$ leading to an increase in the hydrogen generation rate.

Like other investigators, we find that the chemical composition of the metal constituents influences catalytic activity (although the present work on ternary compositions is novel). Table 1 gives the trend of FOMs correlated to single, binary and ternary catalysts for hydrogen generation from $NaBH_4$. The ternary catalyst provides higher FOM than single and binary compositions. A possible conceptual explanation can be that multiplicity of transition metals provide a greater diversity more vacant energy levels in the d-orbitals, where ligands or ions, e.g. $NaBH_4$, $BH_4{}^-$, can attach thereby increasing the time dependent probability of a productive catalytic reaction. For example, the electronic configuration of Pt is [Xe] $4f^{14}$ $5d^9$ $6s^1$, which means that the $BH_4{}^-$ ligand can attach to either one of the vacant sites "s" or "d" orbitals (they require 2 and 10 electrons to be filled). The electronic configuration of Ru is [Kr] $4d^7$ $5s^1$ that means that there are four vacant sites for $BH_4{}^-$ ligand to attach. In summary, a greater diversity in transition metal constituents can give rise to a greater diversity of vacant energy levels where ligands can attach, creating greater number of possibilities for electron transfer via the SiCN/CNT support, thereby enhancing the catalytic activity. A detailed description of the electronic structure of the surface requires *ab initio* calculations that are outside the scope of this paper.

Acknowledgments

Prof. Gialanella is greatly acknowledged for his assistance in TEM observations. The work has been supported by the Dual PhD program between University of Trento, Italy and University of Colorado Boulder, U.S.A. This work is supported by the Ceramics Program in the Division of Materials Research at the National Science Foundation under Grant No.: 0907108.

References

[1] R. Peña-Alonso, A. Sicurelli, E. Callone, G. Carturan, R. Raj, J. Power Sources 165 (2007) 315–323.
[2] B. Sakintuna, F. Lamari-Darkrim, M. Hirscher, Int. J. Hydrogen Energy 32 (2007) 1121–1140.
[3] S.C. Amendola, S.L. Sharp-Goldman, M. Saleem Janjua, N.C. Spencer, M.T. Kelly, P.J. Petillo, M. Binder, Int. J. Hydrogen Energy 25 (2000) 969–975.
[4] N. Patel, B. Patton, C. Zanchetta, R. Fernandes, G. Guella, A. Kale, A. Miotello, Int. J. Hydrogen Energy 33 (2008) 287–292.
[5] J. Zhao, H. Ma, J. Chen, Int. J. Hydrogen Energy 32 (2007) 4711–4716.
[6] J.-H. Wee, K.-Y. Lee, S. Hyun Kim, Fuel Process. Technol. 87 (2006) 811–819.
[7] G.Y. Moon, S.S. Lee, K.Y. Lee, S.H. Kim, K.H. Song, J. Ind. Eng. Chem. 14 (2008) 94–99.
[8] C. Wu, H. Zhang, B. Yi, Catal. Today 93–95 (2004) 477–483.
[9] J.S. Zhang, W.N. Delgass, T.S. Fisher, J.P. Gore, J. Power Sources 164 (2007) 772–781.
[10] S. Özkar, M. Zahmakiran, J. Alloys Compd. 404–406 (2005) 728–731.
[11] C. Wu, F. Wu, Y. Bai, B. Yi, H. Zhang, Mater. Lett. 59 (2005) 1748–1751.
[12] U.B. Demirci, F. Garin, J. Mol. Catal. A 279 (2008) 57–62.
[13] J. Widegren, R.G. Finke, J. Mol. Catal. A: Chem. 198 (2003) 317–341.
[14] A. Garsuch, X. Michaud, K. Böhme, G. Wagner, J.R. Dahn, J. Power Sources 189 (2009) 1008–1011.
[15] J. Shim, K.Y. Joung, J.H. Ahn, W.M. Lee, J. Electrochem. Soc. 154 (2007) B165–B169.
[16] I. Capek, Adv. Colloid Interface Sci. 110 (2004) 49–74.
[17] S.-G. Oh, S.-C. Yi, U.S. Patent no. US 6,660,058 B1, December 9, 2003.
[18] D.V. Goia, E. Matijevic, New J. Chem. (1998) 1203–1215.
[19] A. Nirmala Grace, K. Pandian, Electrochem. Commun. 8 (2006) 1340–1348.
[20] Y. Kojima, Int. J. Hydrogen Energy 27 (10) (2002) 315–323.
[21] N. Patel, Int. J. Hydrogen Energy 33 (2008) 287–292.
[22] U.B. Demirci, J. Mol. Catal. A: Chem. 279 (2008) 57–62.
[23] P. Krishanan, J. Power sources 143 (2005) 17–23.
[24] B.H Liu., J. Alloys Compd. 415 (2006) 288–293.
[25] S.U. Jeong, J. Power Sources 144 (2005) 129–134.
[26] W. Ye, J. Power Sources 164 (2007) 544–548.
[27] J.-H. Kim, Int. J. Hydrogen energy 29 (2004) 263–267.
[28] Y. Liang, H.-B. Dai, Int. J. Hydrogen Energy 35 (2010) 3023–3028.
[29] C.T. Campbell, Science 298 (811) (2002).
[30] L.M. Falicovt, G.A. Somorjait, Proc. Natl. Acad. Sci. U.S.A. 82 (1985) 2207–2211.
[3I] J.M. Thomas, W.J. Thomas, Principles and Practice of Heterogeneous Catalysis, VCH, New York, 1997.
[32] J.H. Sinfelt, Acc. Chem. Res. 10 (1977) 15.
[33] W.H.M. Sachtler, Faraday Dis. Chem. Soc. 72 (1981) 7.
[34] G. Ertl, H. Kntizinger, J. Weitkamp (Eds.), Handbook of Heterogeneous Catalysis, Wiley-VCH, New York, 1997.
[35] G.M. Schwab, Dis. Faraday Soc. 8 (1950) 166.
[36] A. Couper, D.D. Eley, Dis. Faraday Soc. 8 (1950) 172.
[37] D.A. Dowden, P. Reynolds, Dis. Faraday Soc. (1950) 184.
[38] J.K.A. Clarke, Chem. Rev. 75 (1975) 291.
[39] V. Ponec, Adv. Catal. 32 (1983) 149.
[40] J.A. Rodriguez, D.W. Goodman, Surf. Sci. Rep. 14 (1991) 1.
[41] J.A. Rodriguez, Surf. Sci. 345 (1996) 347.
[42] J.A. Rodriguez, Surf. Sci. 318 (1994) 253;
J.A. Rodriguez, Surf. Sci. 303 (1994) 366.
[43] S.R. Shah, R. Raj, J. Eur. Ceram Soc. 25 (2005) 243–249.
[44] S.C. Amendola, P. Onnerud, M.T. Kelly, P.J. Petillo, S.L. Sharp-Goldman, M. Binder, J. Power Source 85 (2000) 186–189.
[45] D. Nagao, Y. Shimazaki, Y. Kobayashi, M. Konno, Colloids Surf. A: Phys. Eng. Asp. 273 (2006) 97–100.
[46] X. Zhang, F. Zhang, J. Mater. Sci. 39 (2004) 5845–5848.
[47] X. Zhang, K.-Y. Chan, J. Mater. Chem. 12 (2002) 1203–1206.

[48] F. Rouquerol, J. Rouquerol, K. Singh, Adsorption by Powders and Porous Solids, Academic Press, San Diego, USA, 1999 (chapter 7).
[49] W. Zhou, Z. Zhou, S. Song, W. Li, G. Sun, P. Tsiakaras, Q. Xin, Appl. Catal. B 46 (2003) 273–285.
[50] A.S.C. Chan, J. Halpern, J. Am. Chem. Soc. 102 (1980) 838.
[51] K.A. Holbrook, P.J. Twist, J. Chem. Soc. A: Inorg. Phys. Theor. 7 (1971) 890–894.
[52] S.C. Amendola, S.L. Sharp-Goldman, M.S. Janjua, M.T. Kelly, P.J. Petillo, M. Binder, J. Power Sources 85 (2) (2000) 186–189.